FINAL REPORT

to

THE OFFICE OF NAVAL RESEARCH

Contract N00014-96-1-09616

May 1996 --- May 1999

ASSERT Grant:

"Evolution of Stress and Damage In Coatings for Thermal Protection Systems"

Professor David R. Clarke

Materials Department, College of Engineering

University of California at Santa Barbara

EXECUTIVE SUMMARY

The scientific goals of this augmentation program were, initially, to establish quantitative relationships between the stress in alumina scales (formed beneath thermal barrier coatings during high-temperature exposure), the oxidation conditions and the accompanying microstructural changes in the scale and the underlying bond coat materials. The technique utilized was that of photostimulated Cr^{3+} luminescence piezospectroscopy developed under the parent grant. As both programs have proceeded and new insights gained, the goal of the ASSERT program has evolved to supply well-characterized TBC coatings for studying damage evolution as well the stress evolution during oxidation.

Piezospectroscopy measurements of the residual stress evolution during prolonged oxidation exposure have revealed that, contrary to expectation in the community, the stress initially changes rather rapidly and then attains a constant value that remains essentially unchanged until failure occurs. Thus, failure is not associated with the residual stress gradually increasing until exceeding some critical stress at which failure occurs. Instead, the observations suggest that damage evolution at the TBC interface occurs until a critical accumulation is reached. The concept that failure may result from damage evolution is borne out by measurements indicating that the spatial variation in residual stress increases with exposure. This work is described in Appendix 1.

The concept that failure of thermal barrier systems results from a progressive development of damage from several individual damage nucleation events, a process that is now widely accepted, focused attention on attempting to identify the microstructural origins of the nucleation sites. Our observations, reinforced by discussions with TBC manufacturers, suggested that one possible origin of defects were regions of local grain misorientation during the initial stages of TBC deposition. For this reason, the research under this grant was redirected towards establishing the relationship between the crystallographic texture of electron beam evaporated zirconia thermal barrier coatings, the effect of the substrate on which they are grown and their thermal conductivity over a range of deposition parameters. The coatings were grown in an electron beam evaporation system at UC Santa Barbara specially modified for the deposition of zirconia thermal barrier coatings. By growing over a range of substrate temperatures upto ~1100°C and on a variety of different substrates coatings with a range of crystallographic texture and densities were produced. In all cases, microstructural analysis reveals that zirconia coatings having a columnar microstructure, similar to those produced by the engine companies. The columnar growth appears to be a consequence of the high deposition rates combined with kinetically limited surface diffusivity since coatings deposited at temperatures in excess of 1100°C and at slow deposition rates were considerably denser and, on single crystal zirconia, were epitaxial. The thermal conductivity measurements of the coatings deposited at 700 C and 1150 were 0.32 W/mK and 1.36 W/mK, respectively. This compares with the thermal conductivity of 2.0 W/mK at room temperature of dense, polycrystalline zirconia. The results of this work are presently being prepared for publication and are described in Appendix 2. The thermal barrier coatings grown under this program have been sent to the Max Planck Institute where their microstructure will be evaluated.

REPORTS OF WORK SUPPORTED UNDER ASSERT GRANT

Appendix 1.

D. R. Clarke, R. J. Christensen and V. K. Tolpygo, **The Evolution of Oxidation Stresses in Zirconia Thermal Barrier Coated Superalloy Leading to Spalling Failure**, Surface and Coatings Technology, **94-95** [1-3] 89-93 (1997).

Appendix 2.

P. Heydt and D. R. Clarke, "**The Effect of Substrate on the Formation of Zirconia Thermal Barrier Coatings**", Journal of the American Ceramic Society, in final preparation.

THE EVOLUTION OF OXIDATION STRESSES IN ZIRCONIA THERMAL BARRIER COATED SUPERALLOY LEADING TO SPALLING FAILURE

D. R. Clarke, R. J. Christensen and V. Tolpygo
Materials Department, College of Engineering,
University of California, Santa Barbara, CA 93106-5050

Abstract

The evolution of the stresses in the aluminum oxide formed beneath a zirconia thermal barrier coating during high-temperature oxidation has been measured from the piezo-spectroscopic shift in the R-line photoluminescence from Cr^{3+} impurities incorporated into the growing aluminum oxide scale. The early stages of oxidation are associated with concurrent phase transformations in the aluminum oxide leading to the stable alpha-alumina phase. On the basis of microstructural observations and the broadening of the luminescence, it is suggested that spalling failure occurs as a result of linking together of localized decohesion of the oxide/bond-coat interface, a process accelerated by moisture enhanced sub-critical crack growth at the interface.

Introduction

Thermal barrier coatings deposited by electron beam evaporation are reported to generally fail on cooling by spalling with separation at the interface with the bond-coat whereas those deposited by plasma-spraying generally fail in the TBC itself. Another characteristic difference is that the coating lifetime is limited by the oxidation kinetics of the bond coat [1]. Whether this is simply a consequence of the fact that electron beam coatings are generally used at significantly higher temperatures, where appreciable oxidation occurs, is not clear but it does emphasize the importance of the thermally grown oxide in determining both the life of the coating and its ultimate failure mode. (The thermally grown oxide is usually aluminum oxide since the bond-coat is aluminum-rich so as to promote the formation of the highly stable oxide as a protective layer.) In this work, we describe measurements of the stress in the thermally grown oxide and its evolution with thermal cycling for one particular TBC/superalloy combination. During the course of these measurements, we have found that there are striking similiarities to the evolution of stress in oxides on many metals which are directly related to the concurrent phase transformations leading to the formation of alpha-alumina that occur during the early stages of oxidation. Also, the rather rare spontaneous spalling of coatings is intimately related to the well-known phenomenon of environmentally assisted slow crack growth at metal/ceramic interfaces.

Oxidation Induced Stresses

Aluminum oxide forms at the interface between the bond-coat and the zirconia thermal barrier coating when oxygen is present. This can occur initially during the deposition of the zirconia coating itself since there is always an activity of oxygen in the deposition chambers usually used and it is also standard practice to deposit in a background of oxygen to ensure the deposition of stoichiometric ZrO_2. Subsequently, whilst the coating provides a thermal barrier during use, it does not block oxidation of the underlying metal because ZrO_2 is a fast oxygen-ion conductor at high temperatures, and as a result more oxide gradually forms, and thickens, at the bond-coat/TBC interface. Although the thickness of the thermally grown oxide is substantially less than that of the TBC, typically only a few microns, it is dense and hence not compliant as is the TBC. As a result the thermal expansion mismatch stress with the bond-coat, and hence the elastic

strain energy in the oxide, can be very high. On the basis of the known thermal expansion coefficients, the compressive stress in the oxide can be of the order of 3-4 GPa on cooling down to room temperature. In addition, by analogy with oxidation of simple metals and alloys, it is expected that additional, growth stresses form in the oxide during high-temperature oxidation. Unfortunately, as the thermally grown oxide is buried beneath the TBC, measurement of the stresses in the oxide has been intractable. However, in recent work, we have shown that the stress can be measured using a non-destructive piezospectroscopic technique [2].

Piezospectroscopic Measurement of Stress

The piezospectroscopic technique is an optical method that utilizes the luminescence from trace Cr^{3+} dopants incorporated into the aluminum oxide formed by oxidation [3]. The luminescence is excited by a laser beam with an energy chosen to penetrate through the zirconia TBC and yet be within the optical absorption band of the chromium-doped aluminum oxide. If the oxide is stressed, the frequency of the Cr^{3+} luminescence shifts from its stress-free value, the piezospectroscopic effect. The frequency shift is related to the stress by the general equation:

$$\Delta\nu_{stress} = \Pi_{ij}\sigma^{c}_{ij} = \Pi_{ij}a_{ki}a_{lj}\sigma_{kl} \qquad (1)$$

where Π_{ij} is the ij-th component of the piezo-spectroscopic tensor and σ^{c}_{ij} is the stress state in the crystallographic basis of the host crystal. In a general coordinate system, the stress state, σ_{ij}, is related to σ^{c}_{ij} by the transformation matrix, a_{ij}. When the alumina is untextured and polycrystalline and a region much larger than the grain size is probed, the frequency shift is proportional to the trace of the stress tensor, namely:

$$\overline{\Delta\nu} = \frac{1}{3}\Pi_{ii}\sigma_{jj} \qquad (2)$$

For a flat alumina scale under biaxial stress, $\bar{\sigma}$, the frequency shift is directly proportional to the stress:

$$\overline{\Delta\nu} = \frac{2}{3}\,\Pi_{ii}\,\bar{\sigma} \qquad (3)$$

The trace of the piezospectroscopic tensor, Π_{ii}, has a numerical value of 7.61 cm^{-1}/GPa for the R2 luminescence [4]. Hence, by measuring the frequency shift, relative to a stress-free, polycrystalline alumina, the biaxial stress can be directly obtained by inverting equation 3.

In making the piezospectroscopic measurements, we have used an argon-ion laser (514nm) to photoexcite the R-line luminescence at 693 nm. Both energies are well below the optical band-gap of partially stabilized zirconia and hence, despite the optical scattering from grain boundaries and porosity, can penetrate through the TBC. (Figure 1). The measurements described in this work were made using an optical microscope-based system with an attached double monochromator and CCD detector for collecting the fluorescence spectrum [3]. The measurements were all made at room temperature. The R-line spectra recorded were subsequently analyzed using a commercially available software package, treating the spectral lineshapes as pseudo-Voigt functions, inorder to determine the frequency shifts.

Results

The R-line luminescence from the thermally grown oxide formed beneath a 140 micron thick electron-beam deposited TBC is shown in figure 2. The luminescence consists of two distinct lines, the R1 and R2 lines. Both are similar to those obtained from oxide scales formed by isothermal oxidation of several alumina-forming alloys, including the same N5 superalloy [3]. The spectra were shifted by several wavenumbers with respect to their stress-free values and both the R1 and R2 lines are significantly broadened. (The broadening is attributed to the existence of strain gradients through the volume of oxide probed by the exciting laser [5].) Similar spectra were recorded from thermal barrier coated samples that were oxidized for different times at 2075°F, and the observed frequency shifts of the R2 line, together with the corresponding biaxial compressive stresses, are reproduced in figure 3.

There are three features of the stresses shown in figure 3 that are similar to those previously reported for the alumina scales formed on thick metals. First, the stresses are almost independent of oxidation time after a transient period. In the oxidation of other metals, notably NiAl, this transient period has been identified as being associated with the transformation from intermediate aluminas to the stable α-Al_2O_3 phase [6]. Second, the magnitude of the stresses is similar to, but larger than, that due to the thermal expansion mismatch strain between polycrystalline aluminum oxide and the superalloy. The difference is attributed to growth stresses. Third, at long oxidation times, the stresses appear to decrease. The cause of this last behavior is not understood but is linked to the onset of decohesion of the oxide scale from the alloys as described qualitatively below.

Phase Evolution Within The TGO

One of the striking findings made during the course of our luminescence studies of TBCs from a number of suppliers and on a variety of different bond-coats has been the wide variation in biaxial stresses, especially at very short oxidation times and indeed before any thermal cycles. In some cases, there is no R-line luminescence after TBC deposition but only develops with oxidation. Together, these observations suggest that there is a phase evolution from an amorphous aluminum oxide to the final, thermodynamically stable alpha-alumina during the early stages of TBC deposition and oxidation. Direct evidence for such an evolution comes the occasional appearance of weak, additional lines in the luminescence spectra after short times. An example is shown in figure 4 where the logarithm of the intensity is plotted against wavenumber, and the weak lines are arrowed. These lines coincide with those now known to be due to Θ-Al_2O_3, one of the transient aluminas formed by heating γ-alumina and which, in turn, transforms to alpha-alumina at still higher temperatures. The presence of spectral lines from both α-Al_2O_3 and Θ-Al_2O_3 in the spectrum of figure 3 indicates that they are co-existing phases in the thermally grown oxide at short oxidation times. This is consistent with X-ray studies of the oxidation of pure NiAl by Brumm and Grabke [7] who identified a region of phase coexistence from about 850 to 1200°C. The picture that then emerges is as follows: On heating up the bond-coated superalloy from room temperature an amorphous aluminum oxide forms on its surface. With continued heating and during deposition and

subsequent high-temperature exposure, the amorphous alumina progressively transforms through a sequence of the transition, metastable aluminas until the alpha-alumina forms. The rate at which this sequence is completed depends in detail on both the activity of oxygen at the different processing steps, as well as time and temperature. Furthermore, it is known that the rates of some of the transformations can be affected by the presence of certain metals, such as Cr and Fe [8].

The consequences of this phase evolution have not been fully explored but two are perhaps pertinent to the life of a TBC coating. Firstly, since the transition aluminas are considerably poorer diffusion barriers than alpha-alumina, the consumption of bond-coat and any diffusional changes established in the underlying superalloy are greater. Secondly, since the molar volume of the alpha-alumina phase is smaller than that of the other transition aluminas, if the phase transition sequence is not complete before the TBC deposition, the phase transformations will be constrained and additional, highly localized stresses generated in the oxide. Whether this is detrimental or not has yet to be established.

Damage Evolution

Examination of the fracture surface revealed by spalling of the TBC indicates that, as described by Meier and Gupta [9], the failure generally occurs in the interfacial region between the spalled TBC and the bond-coat. However, what is rather remarkable is that there can be extensive regions of the fracture in which decohesion apparently occurs at the bond-coat/thermally grown oxide interface, following the detailed oxide grain impressions in the bond-coat. Such regions are joined by fracture in the thermally grown oxide and the TBC but this appears to be where the oxide has grown down along the grain boundaries in the bond-coat. This tentative conclusion needs to be substantiated with further work but highlights the possible role of long-term morphological instability of the oxide/bond-coat interface. Any instability can cause local normal forces to develop across the interface and thereby affect the initiation of interfacial fracture. We believe that the observation that a proportion of the fracture occurs at the oxide/bond-coat interface is of major significance. Since this also occurs when spontaneous, catastrophic spalling failure occurs at room temperature some time

after cooling, it suggests that failure is mediated by environmental-assisted sub-critical crack growth along the metal/ceramic interface. This suggestion is consistent with the fact that alumina/metal interfaces are notoriously prone to moisture enhanced sub-critical crack growth. As our data indicates that the stresses in the thermally grown oxide do not change appreciably with oxidation time, and hence thermal cycles but the life-time does, the question naturally arises as to what actually determines the lifetime. One possibility is that the lifetime is controlled by the initiation of an appropriate interfacial crack. The other is that the initiation step occurs quite quickly and the life is determined by the sub-critical crack growth. In the light of these considerations, it is tempting to suggest that the decrease in biaxial stress at long oxidation times, such as shown in figure 3, is a direct consequence of the growth of decohered regions of the oxide/bond-coat interface. Some, indirect evidence for this comes from the broadening of the R2 luminescence peak as a function of oxidation time, figure 5. (The very large variation at early times is associated with the concurrent phase transformations within the oxide.) The peak broadening is a measure of stress variations within the sample volume probed by the photoexcitation [5], so the observed increase in broadening over the same period as the average biaxial stress decreases is consistent with there being both intact and decohered regions of the interface. Much more study is needed to put these ideas and results on a firmer basis but they provide a working hypothesis to proceed with. This is especially important since the failure interface, being under the TBC, is so inaccessible.

Acknowledgments

This work was supported by the Office of Naval Research under grant N00014-96-1-09616. We are grateful to Ken Murphy, Howmet Corporation, for supplying some of the samples studied.

References

1. R. A. Miller, J. Am. Ceram. Soc., 67 (1984) 517.

2. R. J. Christensen, D. M. Lipkin, D. R. Clarke and K. Murphy, Appl. Phys. Lett. 69 (1996) 3754 .

3. D. M. Lipkin and D. R. Clarke, Oxid. of Metals, 3/4 (1996) 267.

4. J. He and D. R. Clarke, J. Am. Ceram. Soc., 78 (1995) 1347.

5. D. M. Lipkin and D. R. Clarke, J. Appl. Phys., 77 (1995) 1855.

6. D. M. Lipkin, M. Hollatz, M. Bobeth and D. R. Clarke, Corrosion Sci. (in press)

7. M. W. Brumm and H. J. Grabke, Corrosion Sci., 33 (1992) 1677.

8. G. C. Bye and G. T. Simpkin, J. Am. Ceram. Soc., 57 (1974) 367.

9. S. M. Meier and D. K. Gupta, Trans. ASME (1993).

Figure Captions

Figure 1. R-line luminescence from the thermally grown oxide formed at 2075^{o}F after one hour at the interface between an electron-beam deposited TBC and a platinum aluminide coated N5 superalloy.

Figure 2. Schematic diagram of the optical arrangement used to excite, and collect, the R-line from the thermally grown oxide formed beneath the TBC.

Figure 3. The evolution of the piezospectroscopic R-line luminscence shift, and the corresponding biaxial compressive stress, in the thermally grown oxide as a function of oxidation time at 2075^{o}F .

Figure 4. Luminescence from the thermally grown oxide after TBC deposition. In addition to the R-line luminescence from the alpha-alumina phase, there are very weak additional lines (arrowed) due to the co-existence of Θ-alumina. Logarithmic scale.

Figure 5. Full width half maximum breadth of the R2 luminescence line for the same sample and oxidation conditions as that of figure 3.

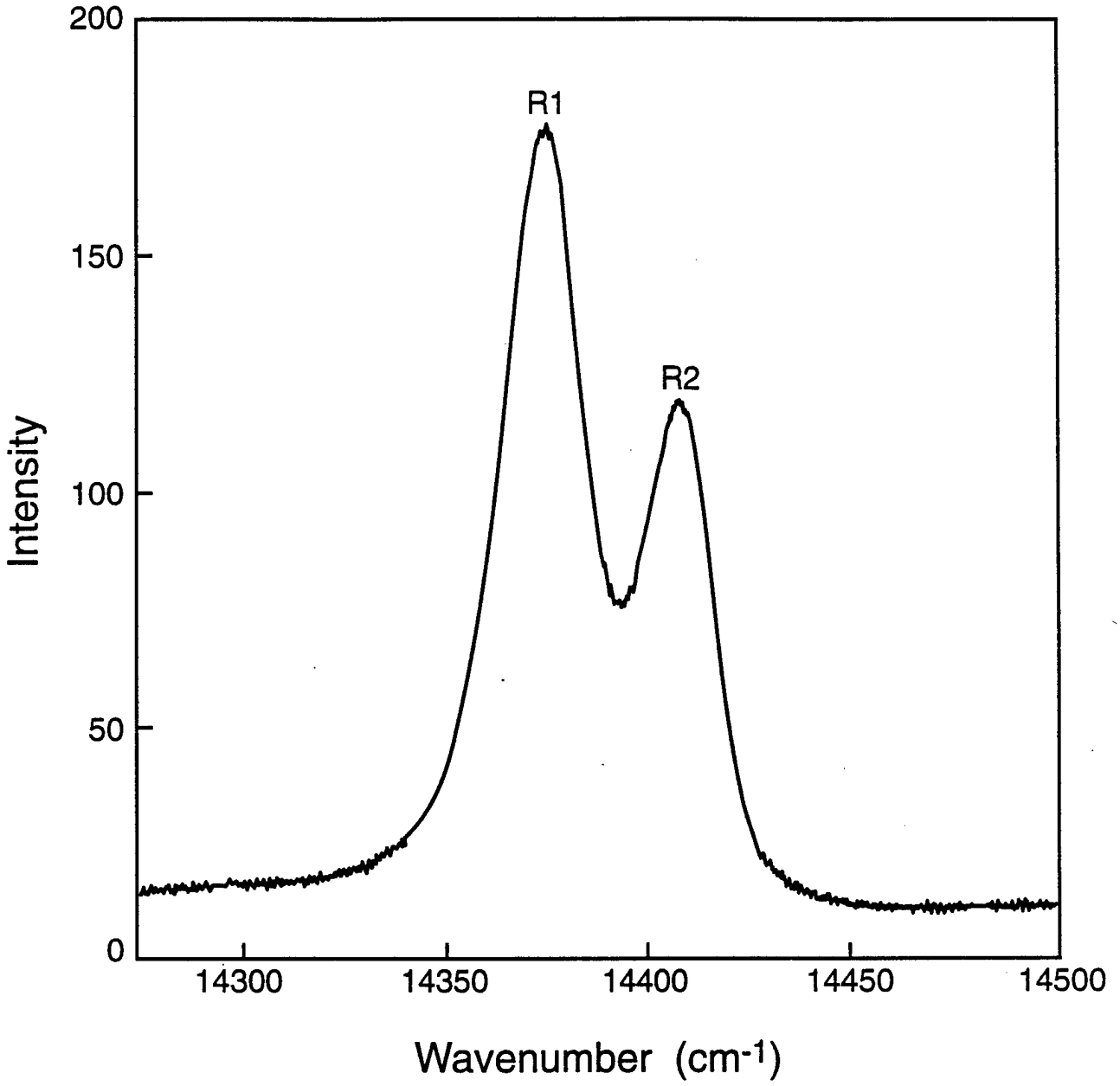

Fig. 1 Clarke et al.

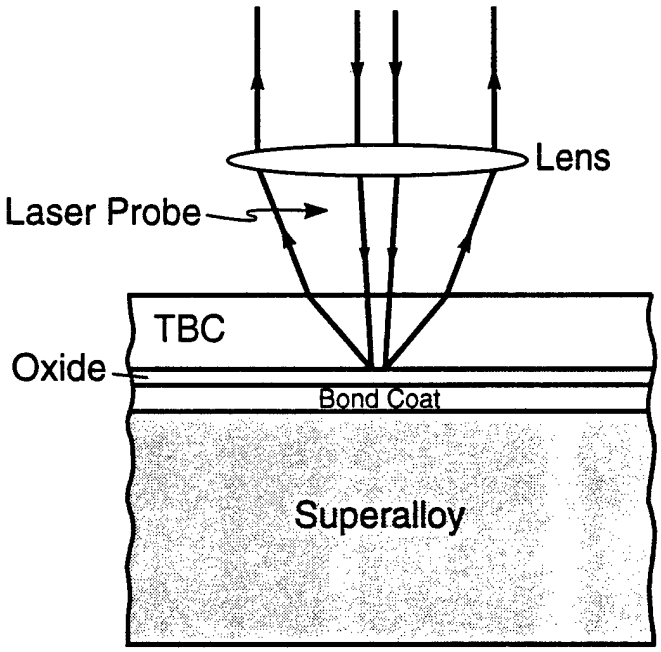

Fig. 2 Clarke et al.

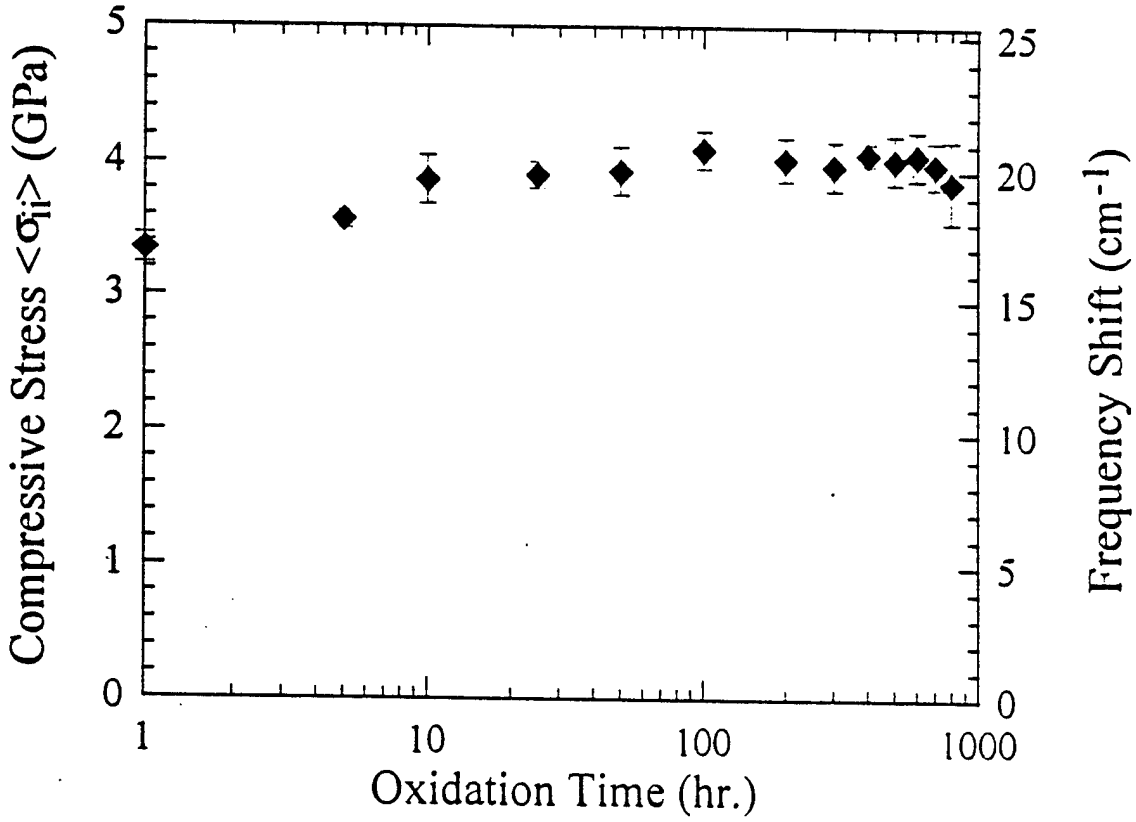

Fig. 3 **Clarke et al.**

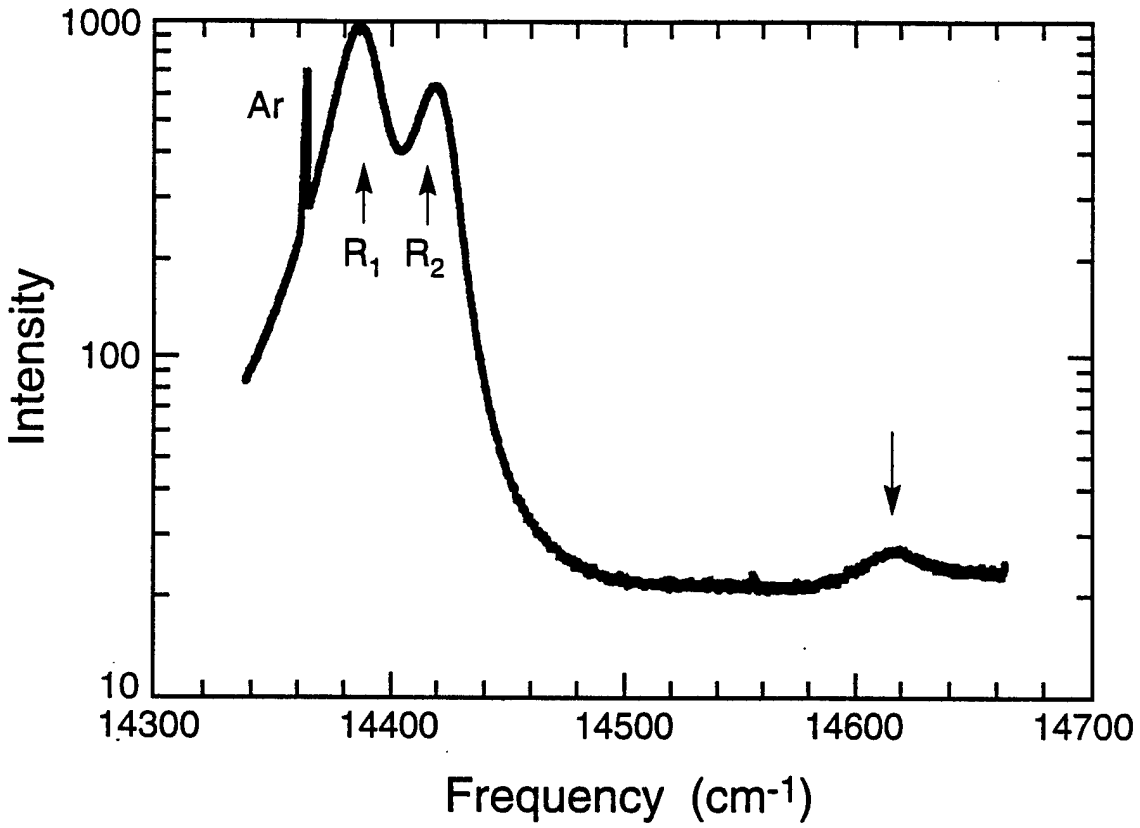

Fig. 4 Clarke et al.

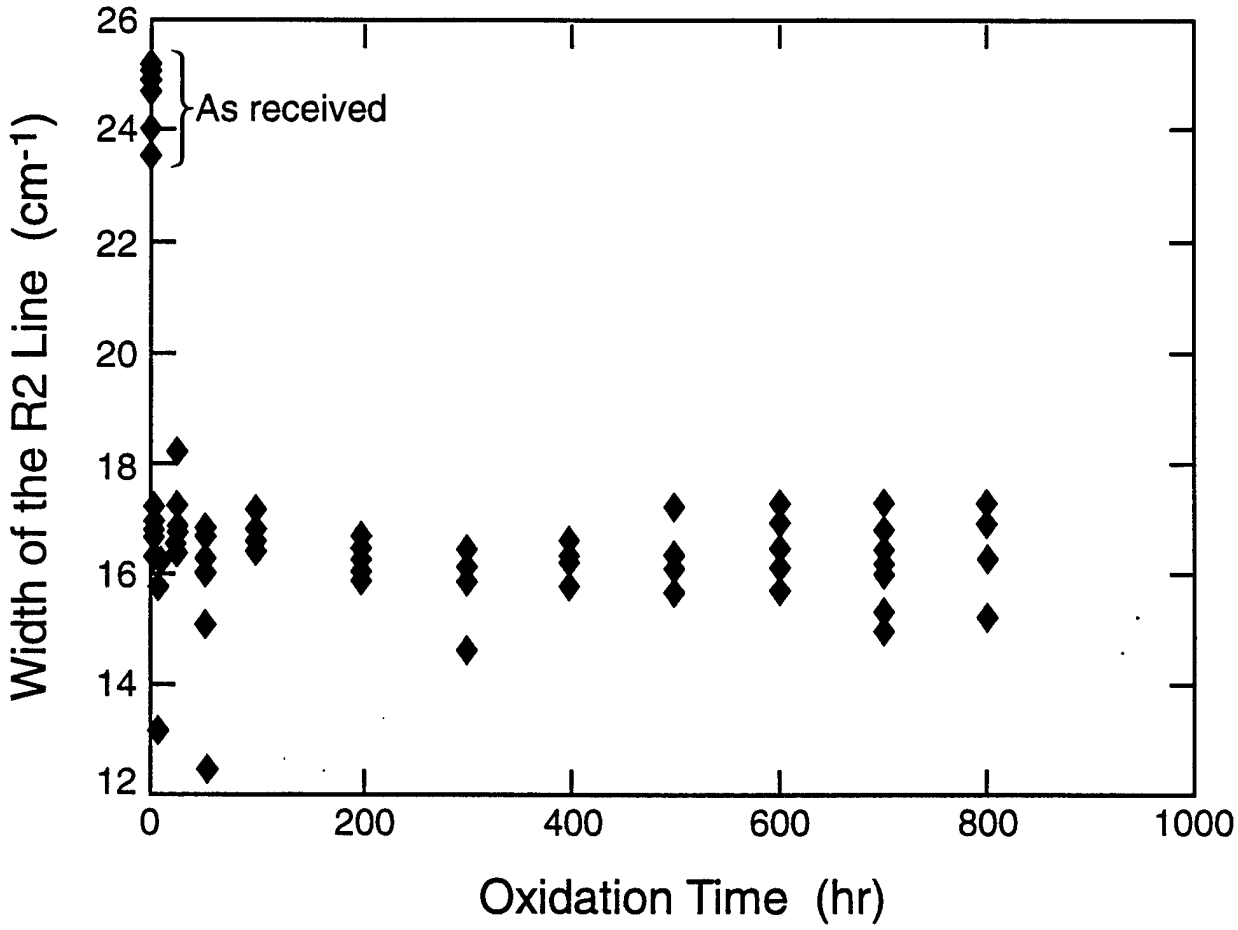

Fig. 5 Clarke et al.

EFFECT OF SUBSTRATE ON ZIRCONIA THERMAL BARRIER COATINGS

P. Heydt, C-Y. Luo and D. R. Clarke
Materials Department, College of Engineering
University of California, Santa Barbara, CA 93106-5050

Abstract

The crystallographic texture and thermal conductivity of zirconia coatings deposited by electron beam evaporation on a variety of substrates have been measured. It is found that the thermal conductivity was independent of whether the coatings were deposited on polycrystalline alumina, single crystal sapphire, single crystal zirconia or fused silica. The thermal conductivity of the coatings deposited at 700°C was 0.32 W/mK, increasing to 1.36 W/mK for coatings deposited at 1150°C. Similarly, the crystallographic texture was also independent of the substrate and had a (111) fiber-texture at 700°C and 900°C switching to a (200) fiber texture by 1050°C. The exception was the coating deposited at 1150°C on (111) single crystal zirconia which was both epitaxial and exhibited a thermal conductivity of 2.46 W/mK. It is concluded that the properties of zirconia thermal barrier coatings are determined by the growth conditions rather than those associated with nucleation on the underlying substrate.

INTRODUCTION

A thermal barrier coating must satisfy two key requirements: a low thermal conductivity perpendicular to the coating, to minimize heat transport through to the underlying alloy, and a low elastic modulus in the plane of the coating to minimize the development of thermal expansion mismatch stresses on cooling. Since porosity is known to decrease both the thermal conductivity and the elastic modulus of materials, both the common methods of depositing coatings in industrial practice, namely electron beam deposition and plasma spraying, are tailored to introduce porosity into the growing coatings. In both methods, the coatings are deposited onto an alloy surface but, in practice the processes used invariably result in the alloy being oxidized prior to the initial deposition of the zirconia coating. Since the majority of alloys on which coatings are deposited are alumina-formers at high temperatures, the oxide formed is usually polycrystalline alumina. However, it is feasible to deposit thin layers of another oxide on the alloy surface or, indeed, use alloys that form alternative oxides when pre-oxidized. As the ideal microstructure of electron-beam deposited coatings consists of columnar grains with both intra- and inter-columnar porosity the question naturally arises as to whether the microstructure is affected by the type and crystallographic nature of the oxide on which the zirconia coating is deposited. In this work, we explore this question by depositing PSZ coatings by electron beam evaporation onto a variety of oxides, including single crystal zirconia, at different temperatures and report both the crystallographic texture and thermal conductivity of the deposited coatings. The single crystal substrates were included in the study to ascertain whether any epitaxial growth of the coating could be attained.

EXPERIMENTAL DETAILS

The coatings were deposited by electron beam evaporation from a commercially available supplier of 7%Y-stabilized zirconia targets. The electron beam deposition system used was one that had been extensively modified so as to deposit thermal barrier coatings onto substrates at different substrate temperatures and at different deposition rates. The design of the deposition system will be described in detail elsewhere [1] but essentially consists of a single 8 kW electron beam that can be focused onto, and rastered across, a circular zirconia billet fed at a constant rate into the deposition chamber. The billet is contained in a water-cooled copper crucible. The deposition rates were measured using a series of quartz crystal oscillators. Oxygen gas could be fed into the chamber during deposition so as to control the stoichiometry of the growing coating. Depositions were generally made in 10^{-4} torr of oxygen and at a rate of 0.5-2.0 μm/min. All the depositions were under normal incidence, stationary substrate conditions. The thickness of the coatings was usually measured from fracture cross-sections using the SEM. All the coating thicknesses were ~ 40 μm unless specifically stated otherwise.

The substrates were obtained from commercial vendors and included polycrystalline alumina, single crystals of zirconia with orientations [110] and [100], [0001] single crystals of sapphire and fused quartz. The zirconia single crystals were stabilized with 9.5 m/o Y_2O_3. Prior to deposition, the substrates were first ultrasonically cleaned in acetone and then isopropanol. After drying they were transferred to the heater assembly and placed into the vacuum system. Following deposition of the zirconia coating the heater was turned off and the sample allowed to cool in the vacuum but with the oxygen flow maintained until 300 °C.

The crystallographic texture of the coatings was determined by X-ray diffraction using Cu Kα radiation. Both standard θ-2θ diffraction analysis was

carried out as well as full texture angular diffraction scans (variable ϕ and ψ) at fixed diffraction angle, θ. The angular scans were recorded from $0<Psi<85^{o}$ at 2.5^{o} intervals and over $0<Phi<360^{o}$ in steps of 2.0^{o}. The angular scans were used to establish the texture of the coatings. Data from the angular scans were used to create 3-D and 2-D diffraction intensity contour scans using IDL software.

The thermal conductivity of the coatings were measured using an electrical third harmonic technique in which a strip-line conductor, deposited on the zirconia coating, is used both as a heater and as a thermal detector. The physical basis of the technique is described in the work of Cahill and Pohl [2]. In essence an alternating current of a frequency ω is passed through the strip line and the voltage generated in the conductor at a frequency of 3ω is measured. By performing the measurements at a series of different frequencies, the thermal conductivity of the material underneath the strip conductor can be ascertained. The methodology, the electrical circuitry and its application to a variety of materials are described in full elsewhere [3,4]. In making the measurements, a number of gold lines of varying width (2, 4, 8 and 16 μm) were deposited on the coatings using standard lithographic techniques in the UCSB clean-room. In order that the lines could follow the rough surface of the coatings, they were made thicker (0.5 μm) than usual for thin films and correspondingly narrower to maintain the required electrical resistance for the third harmonic measurements. For comparison purposes, similar measurements were also made of the single crystal zirconia and sapphire substrates.

OBSERVATIONS

The coatings deposited at 700°C on all the substrates were very similar. They were columnar, had a smooth surface and both the X-ray θ–2θ and full texture scans about the (111) zirconia peak were almost indistinguishable. Figure 1 is the θ–2θ and full texture scan about the (111) zirconia peak for the coating deposited fused quartz indicating that the coatings develop a strong (111) fiber

texture. The fine structure of the columns from the side, in a fracture surface, and looking down onto the top of the coating are shown in figure 2. Distinct differences in the microstructure began to develop at 950°C although the crystallographic texture of all the coatings remained (111) with the exception of that on the sapphire substrate which switched to (200). The coatings on the zirconia and polycrystalline alumina substrates consisted of two co-existing but differently oriented surface grains, even though the X-ray θ–2θ and full texture scans indicated the same (111) fiber texture. On the (100) zirconia substrate, the two apparently competing grain orientations are particularly distinct as shown in figure 3. The individual grains have either a three-fold orientation (either flat or pyramidal) or the "roof-top" morphology, characteristic of many commercial TBCs. The coatings on the sapphire substrate all had the "roof-top" morphology that coarsened at 1050 °C (figure 4). The corresponding X-ray data is shown in figure 5. With the exception of the coatings deposited on (111) zirconia, the crystallographic texture of all the coatings switched to (200) by 1050°C and with the change in texture, the microstructure also changed to a predominately "roof-top" morphology (figure 6). The coatings deposited on the single crystal zirconia substrates at 1150°C exhibited a marked degree of epitaxy with their substrates (figure 7) being particularly strong on the (111) substrate. This was not reflected in any difference in morphology of the columnar grains although it is worth mentioning that one coating deposited on (100) zirconia at 1050°C exhibited an exceptionally flat surface with the only microstructural feature being "etch pits" like features (figure 8).

Despite the obvious differences in the morphology of the individual grains perpendicular to the growth direction, there was little difference in the thermal conductivity of the coatings deposited at the same temperatures. This is seen in the values listed in table 2. Also, shown in the table are values of the thermal conductivity of a variety of other forms of zirconia for comparison purposes. The striking features of the measured thermal conductivity are the very low values of the coatings deposited at 700°C, the increase to a value typical of commercial EB-

PVD coatings at 1150°C and the value of the epitaxial coating on the (111) zirconia substrate. The last is larger than that of dense polycrystalline zirconia but still considerably less than that of single crystal zirconia.

DISCUSSION AND CONCLUSIONS

The observations described in this work clearly show that the crystallographic texture, the average column size and, most importantly, the thermal conductivity of thick, electron-beam evaporated zirconia coatings are almost independent of the substrate on which they are deposited. The one exception appears to be when the zirconia is grown on (111) single crystal of cubic zirconia at a temperature of 1150°C. In this particular case, the zirconia appears to have grown epitaxially on the substrate, preserving the (111) single crystal orientation and exhibiting a higher thermal conductivity (~2.5 W/mK) than polycrystalline zirconia. The obvious conclusion to be drawn from these observations is that, at least over the temperature range and deposition rates used, the microstructural and crystallographic development of the coatings is determined by the deposition and growth conditions and not by any crystallographic relation, including possible epitaxy, with the substrate material. Since the thermal conductivity of the coatings are all substantially smaller than that of either single crystal or dense polycrystalline zirconia, the coatings must contain a substantial fraction of porosity even in those coatings, such as that grown on sapphire, where the microstructure appears quite dense. This fact and the observation of columns indicates that under the deposition condition used, the rate of deposition must be much larger than the rate of thermal smoothing due to surface diffusion. Under such conditions, both computer simulation [5,6] as well as simple geometric arguments indicate that, the microstructural development is the result of two phenomena. The first is simply that in the absence of appreciable re-evaporation from the growing surface, the growth direction is dictated by the direction of the incoming flux of zirconia. The second

is that in a competition between crystals growing at different rates, the fastest growing orientation taking over and dominates the crystallographic texture. This appears to be the case for all the coatings investigated in this work with the exception, as remarked above, of that grown on (111) zirconia. The fiber texture of all the coatings at 700, 950 and 1050°C, further indicates that the fastest growing grains had no preferred crystallographic orientation with the underlying substrate. The switch in texture from a predominately (111) fiber texture at lower substrate temperatures to a (200) fiber texture at the higher temperatures is consistent with previous observations although this work does not provide any new insight as to the origin of the transition to the (200) texture.

As pointed out in the previous section, the substantially lower thermal conductivity of the coatings than that of single crystal zirconia, indicates that they must contain substantial fractions of porosity. No pores were large enough to be visible in the fracture cross-sections suggesting that they are of microscopic size and attempts to make them more evident by polishing the cross-sections were unsuccessful due to smearing of the zirconia on polishing. Transmission electron microscopy observations are underway to measure the pore size and to investigate the transition region, near the zirconia substrates, were the transition to a columnar morphology occurs. However, these observations are not necessary to conclude that the bulk of the porosity must be incorporated into the individual columnar grains as they grow.

The significance of this work is the demonstration that the columnar structure of zirconia TBCs is a consequence of the imposed, highly directed growth of the coating and that the nucleation of the TBC on the substrate is of minor importance. This is borne out by the fact that the columnar structure is achieved irrespective of whether the substrate is amorphous, polycrystalline, single crystalline or even lattice matched. The relative insensitivity of the thermal conductivity of the coating to the nature of the substrate, except for the epitaxial growth on (111) zirconia, also suggests that it is the growth not the nucleation process that is of primary importance. The significantly higher

conductivity at the higher deposition temperature is consistent with the idea that the incorporation of porosity is intimately related to the temporal competition between surface diffusion on the growing surface, which will tend to close up pores, and the rate at which new material is being deposited on the growing surface. However, it is also consistent with a contrasting idea that the incorporation of porosity is relatively temperature independent but that porosity coarsening is highly temperature dependent such that at the higher deposition temperatures, pores trapped earlier coarsen during the subsequent deposition of the coating. This will be testable by TEM observations underway.

ACKNOWLEDGMENT

The authors are grateful to the Office of Naval Research for support of this work through an ASSERT grant number N00014-96-1-0916. It is also a pleasure to acknowledge the assistance of Mr. D. Stave and discussions with both S. Terry and Professor Carlos Levi.

REFERENCES

1. D. Stave, S. Terry and C. Levi, to be published
2. D. G. Cahill and R. O. Pohl, Physical Review B, **35** 4067-4073 (1987).
3. Q. Wen and D. R. Clarke, Journal of Applied Physics, **83** 1132 (1998).
4. C. Luo, H. Marchant, S. DenBaars and D. R. Clarke, Applied Physics Review, submitted for publication.
5. Muller, Journal of Applied Physics,
6. M. Pusch, C. Levi and D. R. Clarke, to be published

FIGURE CAPTIONS

Figure 1. θ–2θ and full texture scan about the (111) zirconia peak of a zirconia coating deposited at 700 °C on fused quartz.

Figure 2. Microstructure of a zirconia coating deposited at 700°C on fused quartz. The fine columnar structure is seen in the fracture cross-section (a) and the fine structure of the growth surface is seen in plan view (b).

Figure 3. (a) Growth surface of a zirconia coating deposited at 950°C on (100) zirconia illustrating two principal distinct but co-existing populations of grain morphology. One, has three-fold rotational symmetry (with either pyramidal or flat-top morphology) (b) whilst the other has the "roof-top" morphology (c).

Figure 4. Growth surface of coating formed at 1050 °C on sapphire illustrating the "roof-top" morphology.

Figure 5. θ–2θ and full texture scans about the (200) zirconia peak of a zirconia coating on sapphire deposited at 1050°C

Figure 6. Growth surface illustrating the "roof-top" morphology typical of the coatings formed on all the substrates at 1150°C. This was formed on (100) zirconia.

Figure 7. θ–2θ and angular scans for coatings deposited on (100) and (111) zirconia single crystal substrates at 1150°C. The scans were about the (100) and (111) diffraction peaks for the (100) and (111) substrates, respectively.

Figure 8. Growth surface on coating deposited on a (100) zirconia substrate at 1050°C. This surface was remarkable in that it was completely flat other than the "etch-pit" like features shown here.

Table I.

The Crystallographic Fiber Texture of The Coatings

Substrate	Substrate Temperature			
	700°C	950°C	1050°C	1150°C
Fused Quartz	(111)	----	----	----
Polycrystalline Alumina	(111)	(111)	(200)	(200)
[0001] Sapphire	(111)	(200)	(200)	(200) Strong (111) Weak
(111) Zirconia	(111)	(111)	----	(111)*
(100) Zirconia	(111)	(111)	(200)	(200)** Strong (111) Weak

*Epitaxial rather than fiber textured.
** Weakly epitaxial

Table 2.

Thermal Conductivity

Form of Zirconia	Thermal Conductivity W/mK	Measurement Technique	Reference
Single crystal		Laser Flash	
Single crystal		3 ω	This work
Polycrystalline Bulk	2.0	Laser flash	
Polycrystalline Bulk	2.0	3ω	This work
Plasma sprayed	1.2	Laser flash	
EB-PVD commercial		Laser flash	
EB-PVD at 700°C **	0.35	3ω	This work
EB-PVD at 1150°C ***	1.36	3ω	This work
EB-PVD at 1150°C on (111) ZrO_2	2.46	3ω	This work

** On fused quartz, polycrystalline alumina, (0001) sapphire, (100) and (111) zirconia

*** On polycrystalline alumina, (0001) sapphire and (100) zirconia

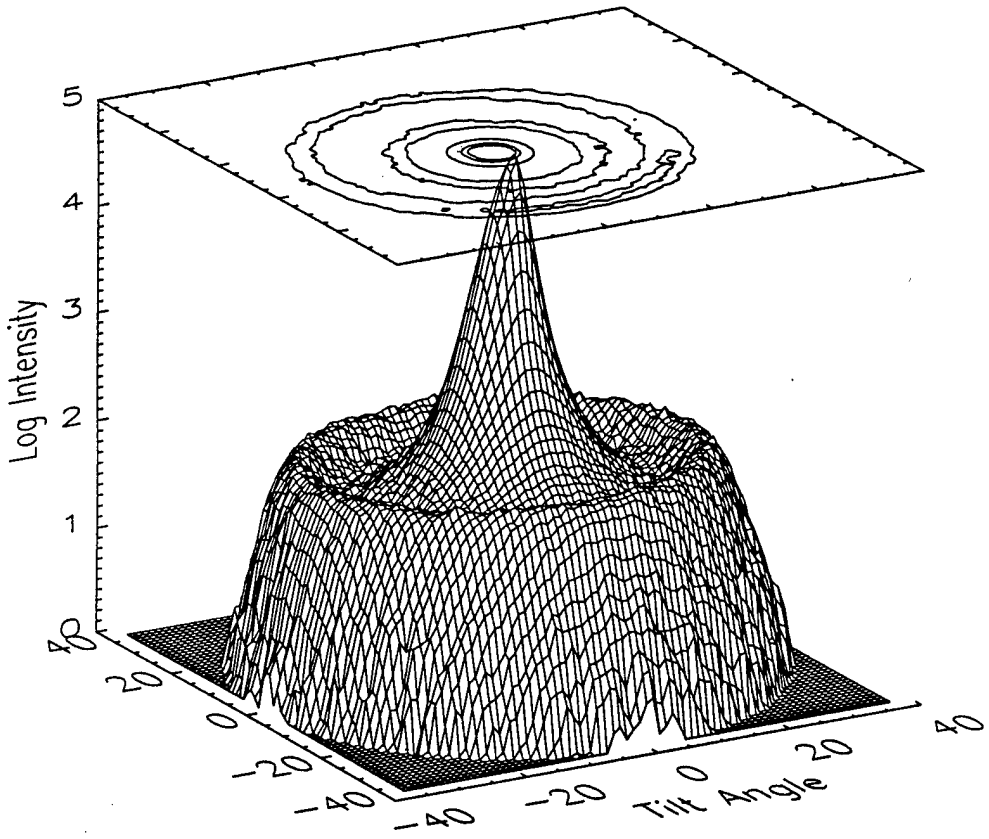
Log Intensity
5
4
3
2
1
0
40
20
0
-20
-40
-40
-20
0
20
40
Tilt Angle

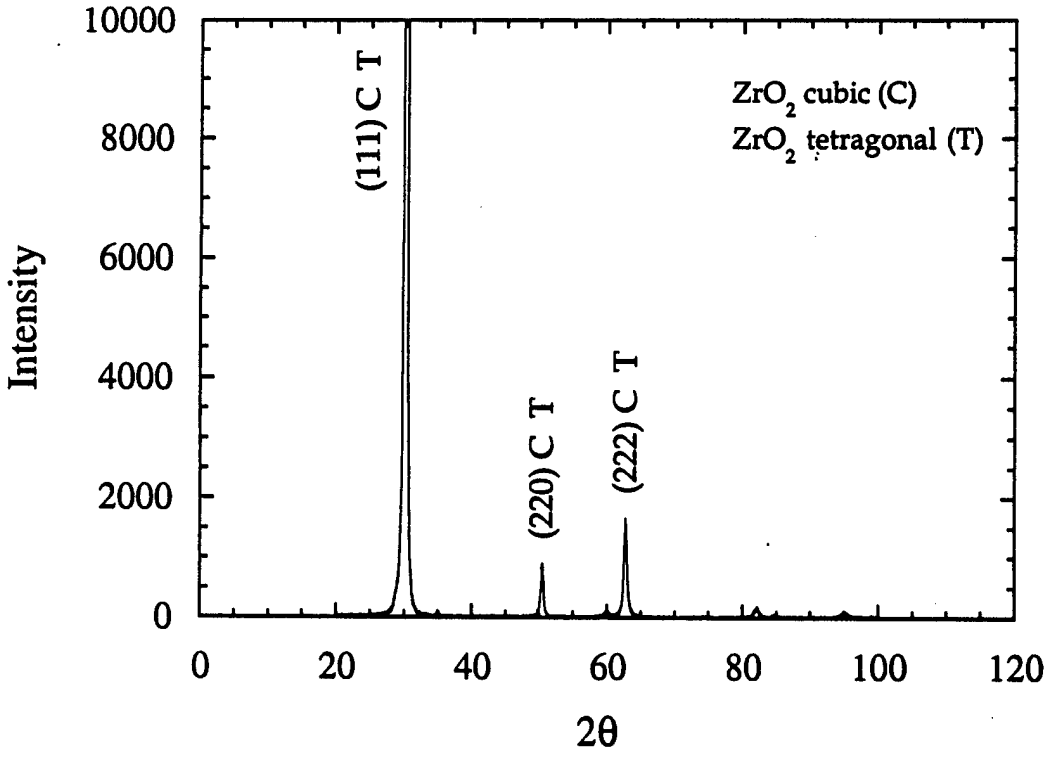
Intensity
10000
8000
6000
4000
2000
0
(111) C T
(220) C T
(222) C T
ZrO2 cubic (C)
ZrO2 tetragonal (T)
0
20
40
60
80
100
120
2θ

Figure 1

70 SX 01 01

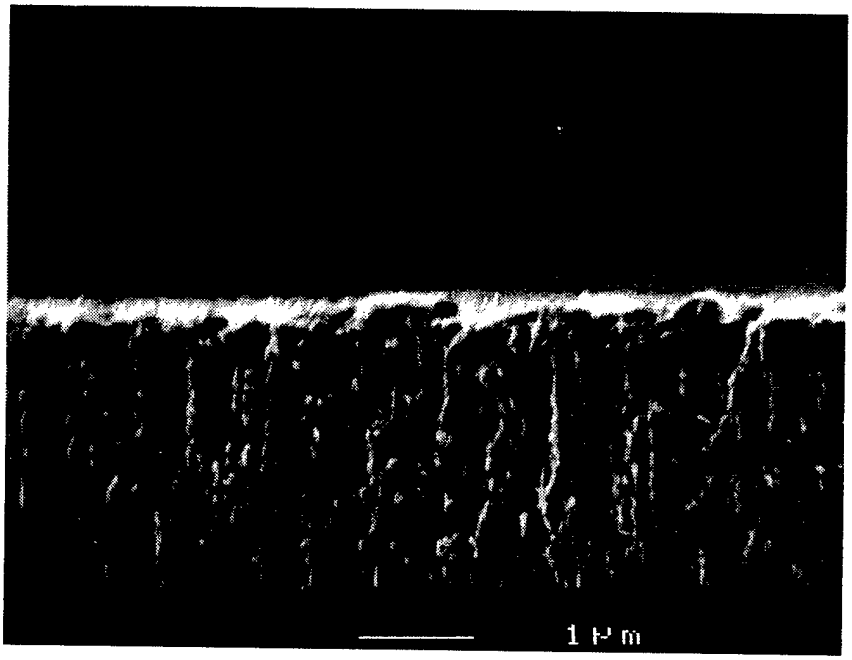

Figure 2 (a)

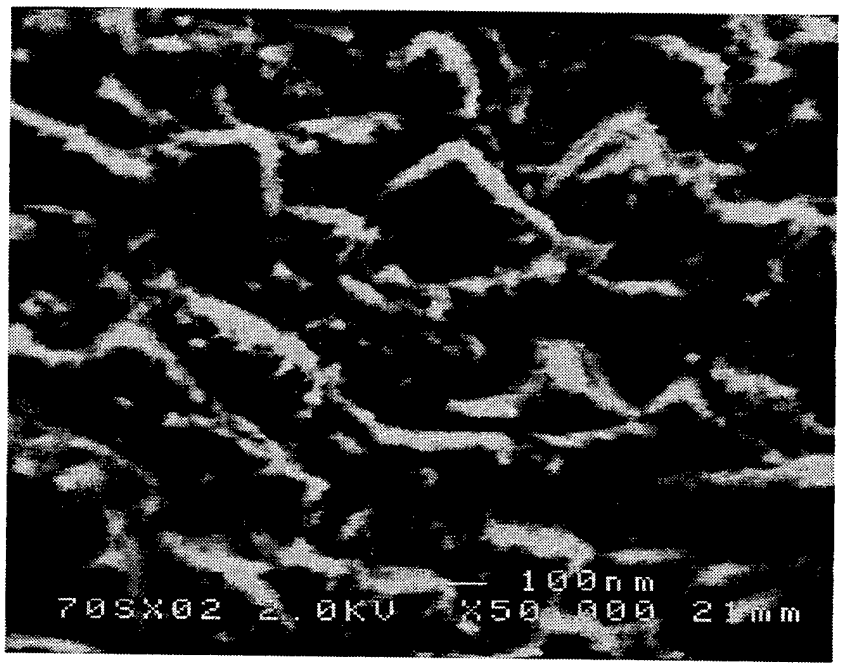

Figure 2 (b)

95 ZX 0101 C

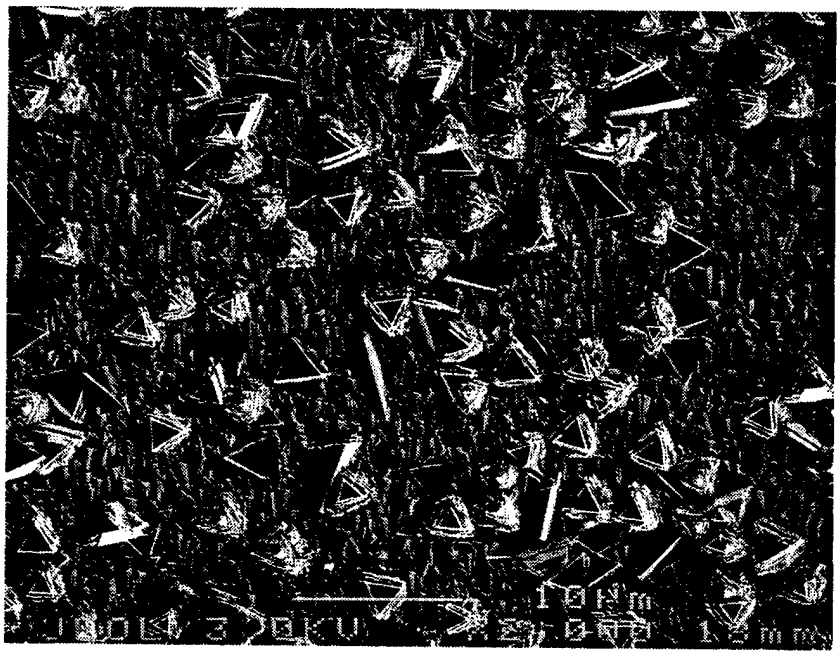

Figure 3 (a)

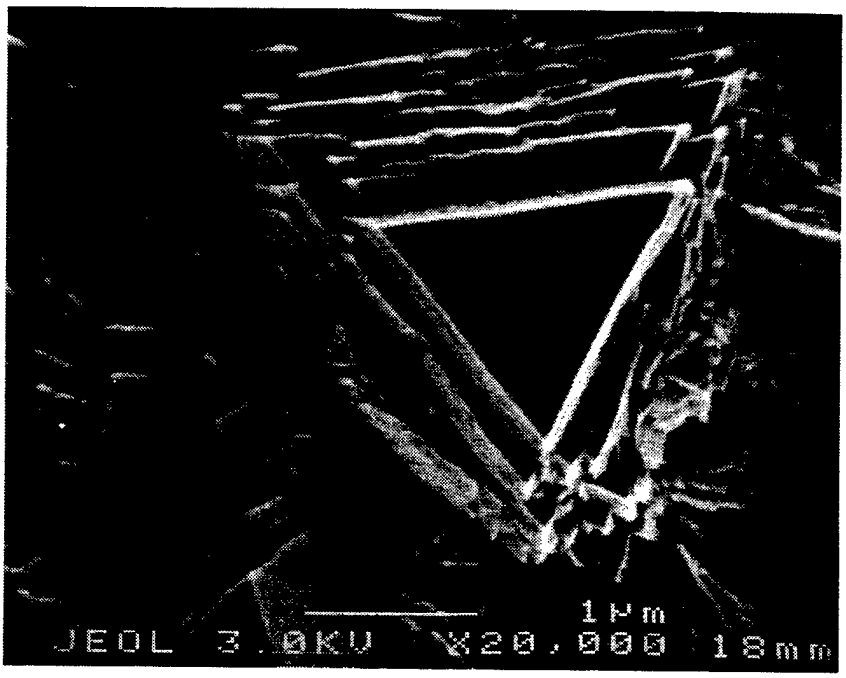

Figure 3 (b)

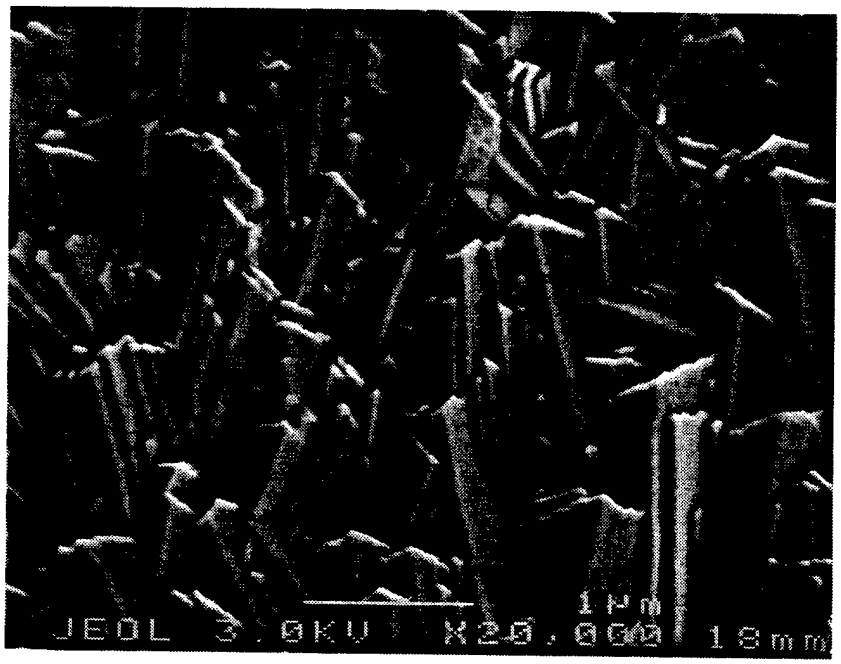

Figure 3 (c)

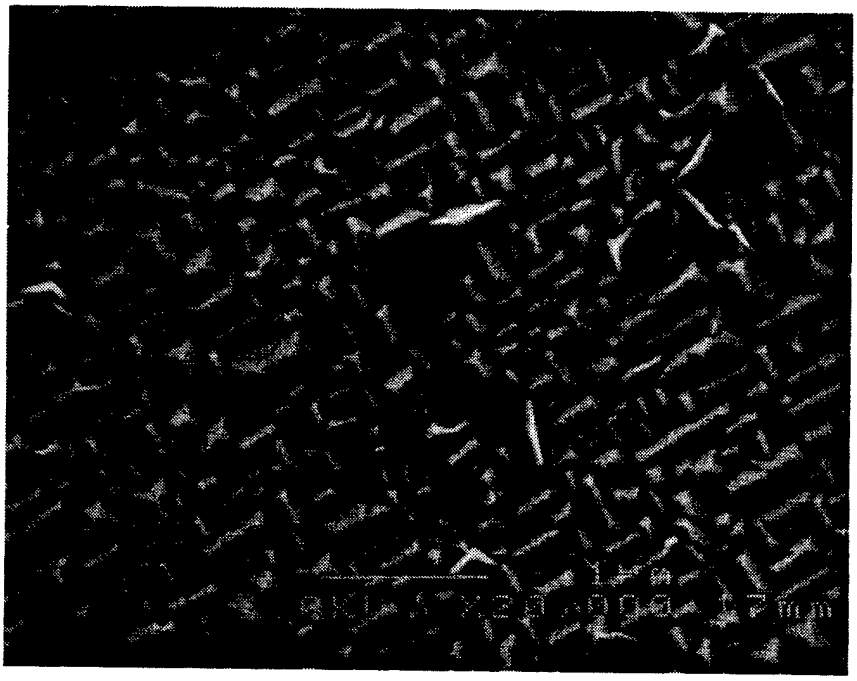

Figure 4

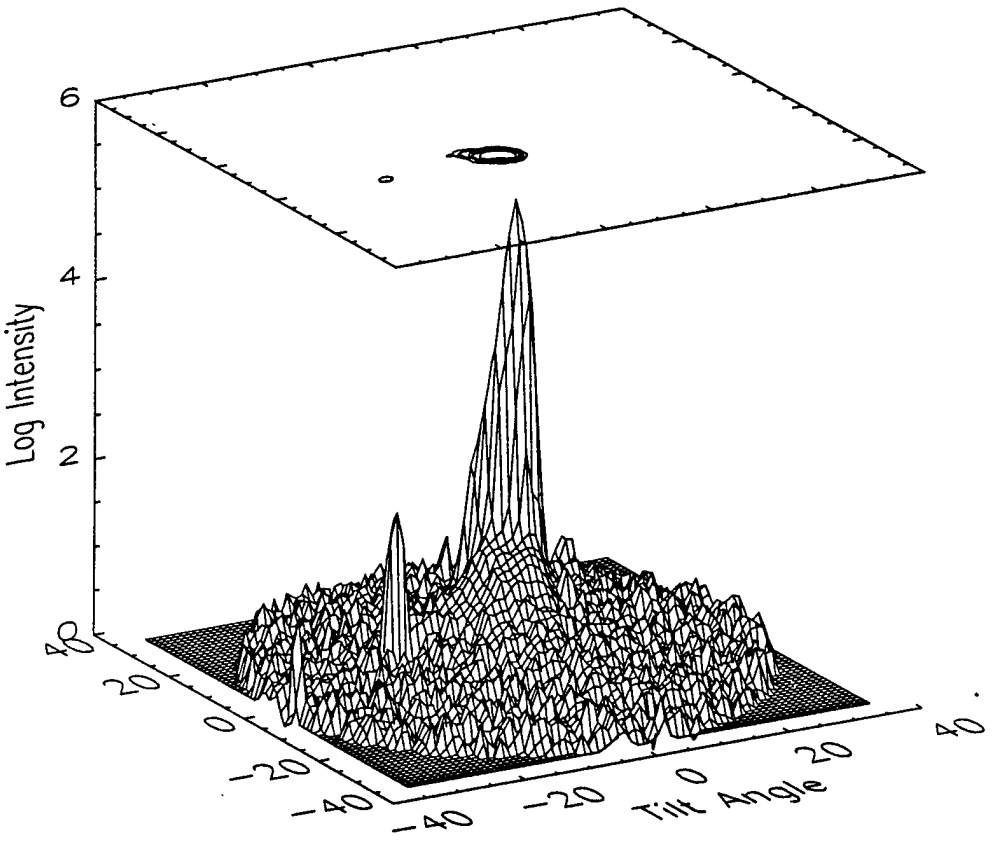
Log Intensity
6
4
2
0
40
20
0
-20
-40
-40
-20
0
20
40
Tilt Angle

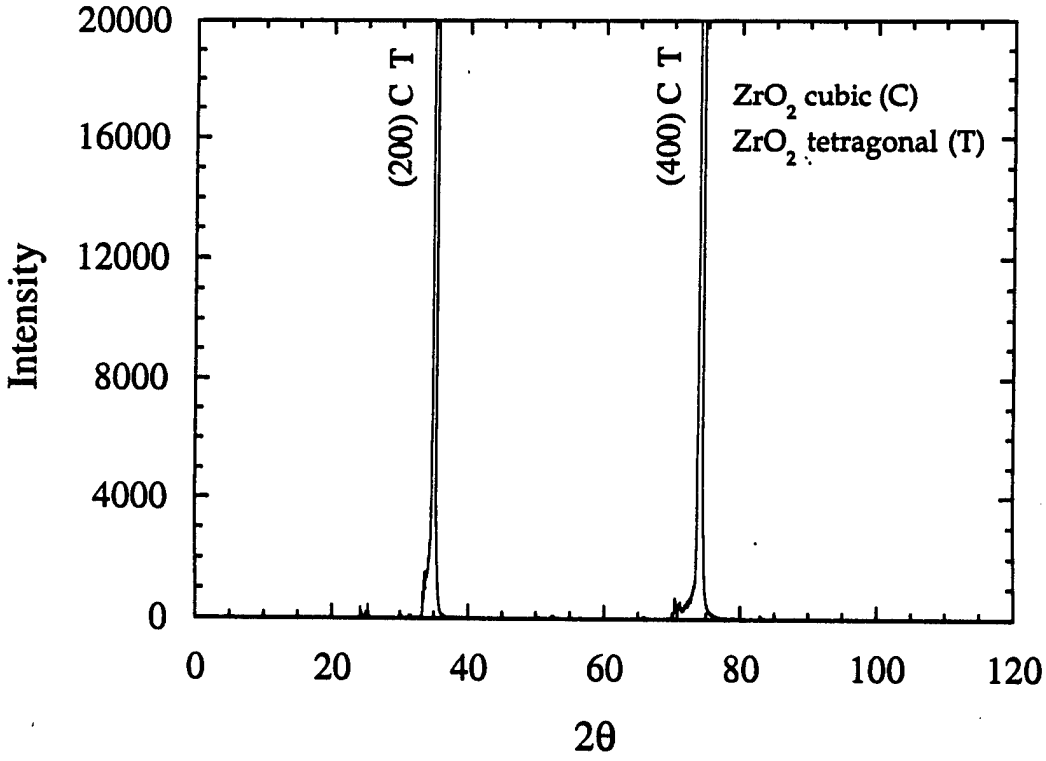
Intensity
20000
16000
12000
8000
4000
0
(200) C T
(400) C T
ZrO2 cubic (C)
ZrO2 tetragonal (T)
0
20
40
60
80
100
120
2θ

Figure 5

11 SX 0101 ~

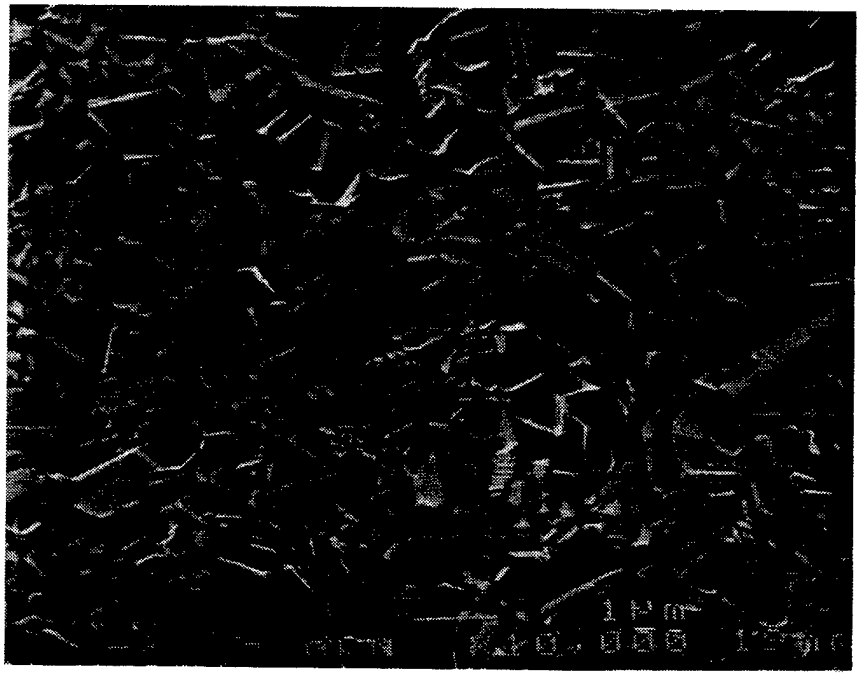

Figure 6

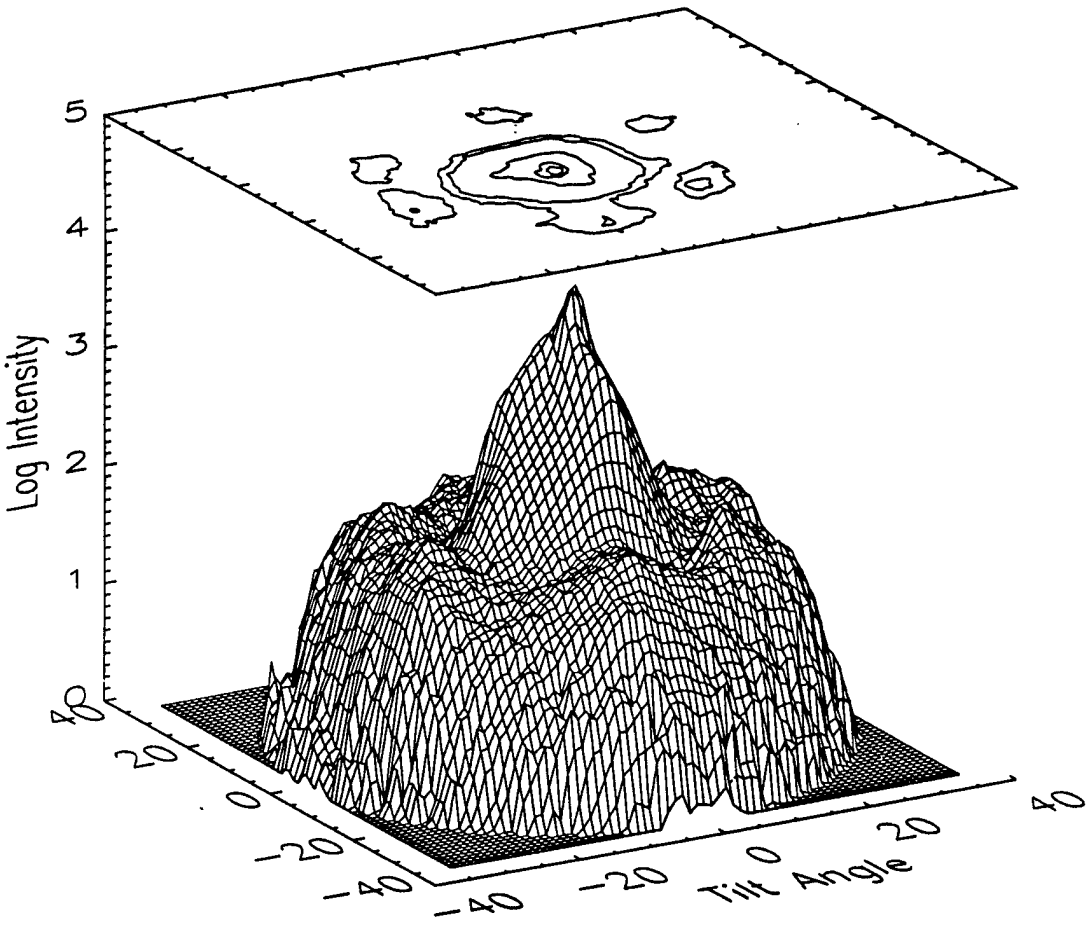
Log Intensity
5
4
3
2
1
0
40
20
0
-20
-40
-40
-20
0
20
40
Tilt Angle

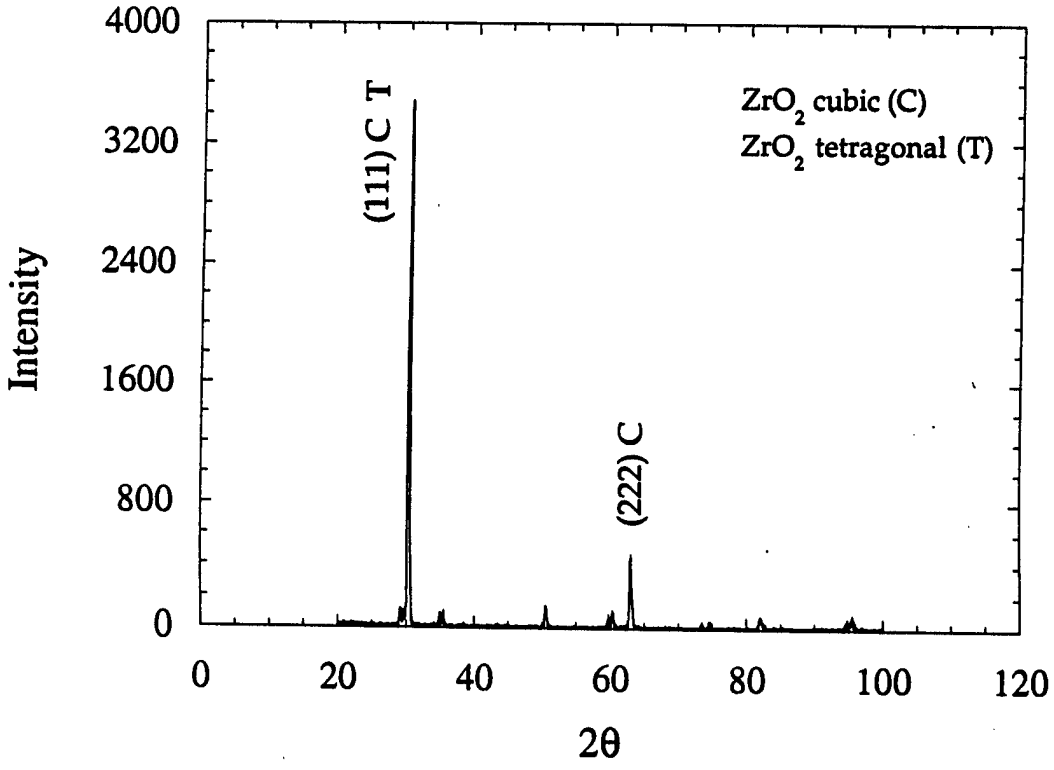
Intensity
4000
3200
2400
1600
800
0
(111) C T
(222) C
ZrO2 cubic (C)
ZrO2 tetragonal (T)
0
20
40
60
80
100
120
2θ

Figure 7

10 ZX 0101

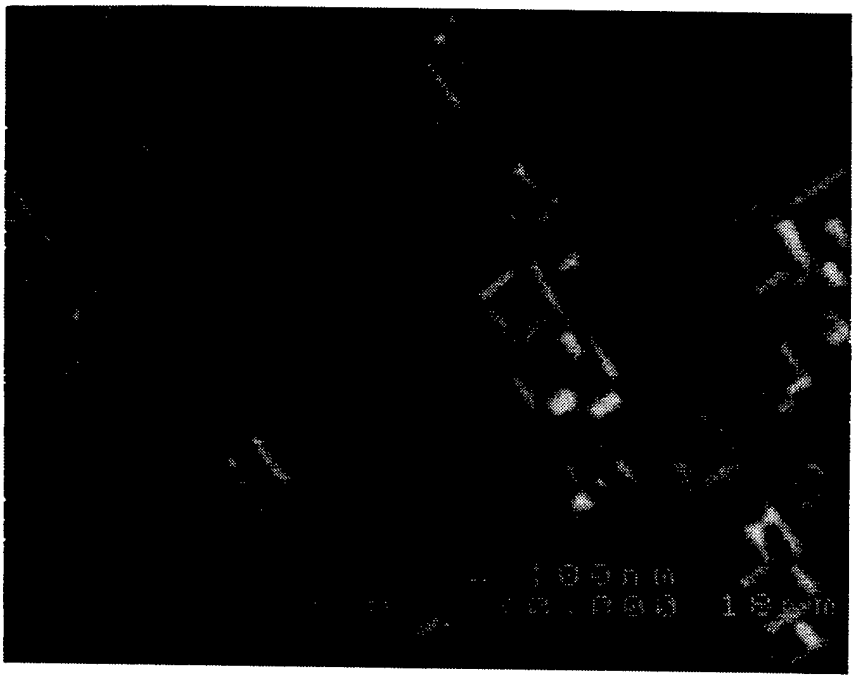

Figure 8

REPORT DOCUMENTATION PAGE

Form Approved
OMB No. 0705–0188

1. AGENCY USE ONLY (Leave blank)	2. REPORT DATE	3. REPORT TYPE AND DATES COVERED
		Final Report 6/1/96 through 5/31/99

4. TITLE AND SUBTITLE
ASSERT Grant: Evolution of Stress and Damage in Coatings for Thermal Protection

5. FUNDING NUMBERS
N00014-96-1-0916

6. AUTHOR(S)
David R. Clarke

7. PERFORMING ORGANIZATION NAME(S) AND ADDRESS(ES)

Materials Department
College of Engineering
University of California
Santa Barbara, CA 93106-5050

8. PERFORMING ORGANIZATION REPORT NUMBER
8-442490-25831

9. SPONSORING/MONITORING AGENCY NAME(S) AND ADDRESS(ES)

Office of Naval Research
Program Officer : Dr. S. G. Fishman
Ballston Centre Tower One
800 North Quincy Street
Arlington, VA 22217-5660

10. SPONSORING/MONITORING AGENCY REPORT NUMBER

11. SUPPLEMENTARY NOTES

DISTRIBUTION STATEMENT A
Approved for Public Release
Distribution Unlimited

12A. DISTRIBUTION/AVAILABILITY STATEMENT

12B. DISTRIBUTION CODE

13. ABSTRACT (Maximum 200 words)

The goals of this AASERT were to establish quantitative relationships between the stress in alumina scales (formed beneath thermal barrier coatings during high-temperature exposure), the oxidation conditions and accompanying microstructural changes. The technique utilized was that of photostimulated Cr^{3+} luminescence piezospectroscopy developed under the parent grant. Piezospectroscopy measurements of the residual stress evolution during prolonged oxidation exposure have revealed that, contrary to expectation in the community, the stress initially changes rather rapidly and then attains a constant value that remains essentially unchanged until failure occurs. Thus, failure is not associated with the residual stress gradually increasing until exceeding some critical stress occurs. Instead, as both programs proceeded it became clear that failure usually occurs by a progressive failure mode, one in which localized regions of damage nucleate, then grow until finally linking up to form a critical-sized defect that can cause spalling. From this new insight, a detailed investigation was made into the microstructural origins of possible nucleating defects, in particular those associated with the early stages of deposition of zirconia TBC coatings. The microstructure and crystallographic texture of thermal barrier coatings deposited on a variety of substrates was investigated and related to the thermal conductivity of the coatings.

14. SUBJECT TERMS	15. NUMBER OF PAGES
	16. PRICE CODE

17. SECURITY CLASSIFICATION OF REPORT	18. SECURITY CLASSIFICATION OF THIS PAGE	19. SECURITY CLASSIFICATION OF ABSTRACT	20. LIMITATION OF ABSTRACT
Unclassified	Unclassified	Unclassified	